Nuclear Materials and Energy 25 (2020) 100776

Contents lists available at ScienceDirect

Nuclear Materials and Energy

journal homepage: www.elsevier.com/locate/nme

Indentation testing on 3 MeV proton irradiated tungsten

R. Rayaprolu[a,*], S. Möller[a], R. Abernethy[b], M. Rasinski[a], J.C. Haley[c], Ch. Linsmeier[a]

[a] Forschungszentrum Jülich GmbH, Institut für Energie- und Klimaforschung – Plasmaphysik, 52425 Jülich, Germany
[b] Culham Centre for Fusion Energy, Culham Science Centre, Abingdon, Oxfordshire OX14 3DB, United Kingdom
[c] University of Oxford, Department of materials, Oxford OX1 3PH, United Kingdom

ARTICLE INFO

Keywords:
Tungsten
Neutron damage
Proton damage
3 MeV protons
Instrumented indentation
TEM
Nano indentation
Ion damage

ABSTRACT

Tungsten samples have been irradiated with 3 MeV protons with dose rates of 1×10^{-04} to 5×10^{-05} dpa/s to doses of 0.01–0.67 dpa at 360 K in a pilot experiment. Micro- and macro-indentation were used to measure irradiation hardening in the samples. An initial irradiation hardening of 1.23 $\pm$ 0.09 GPa and 1.88 $\pm$ 0.83 GPa was measured by micro and macro indentation. The irradiation hardening was observed to saturate at 0.03 dpa damage. Dislocation loops were identified using TEM suggesting an increasing loop size with dose.

1. Introduction

As the plans for the demonstration fusion reactor mature [1,2], material technology is seen to be a key player [3]. High heat fluxes between 10 and 20 MW/m^2 along with transient thermal loads [4,5], considerable neutron damage at rates of 3 −4 dpa/year [6] and steady impacting plasma loads pose a triple threat to the plasma facing material (first wall). Tungsten (W) is a forerunner for the first wall given its high melting point (3695 K), high thermal conductivity and reltively low sputtering [7,8]. Infact novel solutions with W, such as W-fiber components, mixed W-Cr-Ti alloys and functionally graded layers of W and Cu are being proposed as solutions for handling the triple threat of plasma, neutron and heat loads [9]. Recently a large emphasis has been on collecting data to understand the irradiation damage and on post irradiation engineering properties using fission reactors [10] and heavy ion irradiations [11,12].

The unavailability of fusion neutron sources such as IFMIF [13] for material qualification post neutron damage has led to long irradiation campaigns at fission reactors. However in view of the long cycle times and higher than fusion transmutation component, accelerators have led the way to understand and quantify effects of neutron damage in materials [14]. Accelerator irradiation are often performed using heavy ions such as ‘Au+’ or self ions such as ‘W+’ ions on ‘W’ [15–17]. The heavy ions have low penetration depths and create damage close to the surface, within the 2 μm where implantation and surface damage effects can be observed.

Another approach towards emulating neutron damage using accelerator irradiation is to use low energy light ions such as 3 MeV protons [18,19]. The penetration depth of protons is much higher than heavy ions and an attempt to study macroscopic changes can be undertaken. The comparison of proton irradiations to heavy ions and neutrons is well documented [20] and while low energy protons produce scattered dislocation cascades, they have been used to simulate reasonable dose rate conditions to mimic neutron irradiation effects [19]. Low energy proton irradiation shares the benefit with heavy ion irradiation of avoiding activation of the sample, allowing analysis using non-active laboratory facilities. Higher energy protons using 16 & 30 MeV protons from a cyclotron was detailed in our previous publication [21], which produces similar to fusion a displacement and transmutational component and has a lower cycle time than fission reactors. However, similar to fission, the samples are radioactive and require hot cells with additional radiation safety requirements.

A recent transmission electron microscopy(TEM) study in tungsten using proton energies of 40 keV(in situ) and 3 MeV(ex-situ) at 623 K determined the damage structures resulting from the proton irradiation at doses of 0.1–0.7 dpa [18]. The in situ observation results showed that a/2 < 111 > dislocation loops had formed and that loop size increased with dose but loop density was observed to decrease up to 0.7 dpa. However, different dislocation structures were found after ex-situ irradiated samples. This suggests that the free surfaces present or low ion energies used during the in situ TEM irradiation may be affecting the microstructure development.

Through the years of fusion research, small scale testing techniques has been constantly discussed and evolved [22–24]. Instrumented

* Corresponding author.

https://doi.org/10.1016/j.nme.2020.100776
Received 10 March 2020; Received in revised form 27 May 2020; Accepted 13 July 2020
Available online 07 August 2020

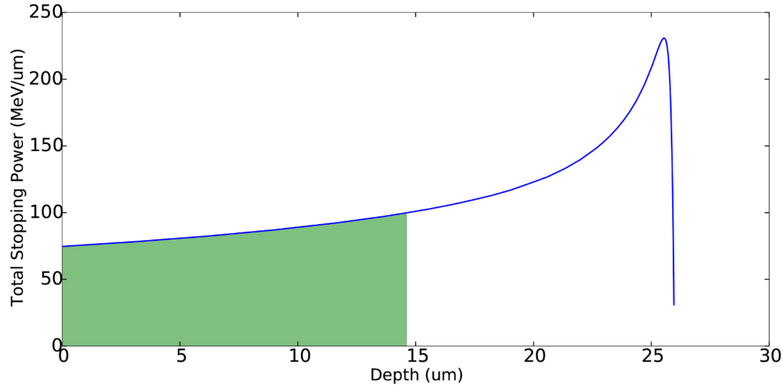

(a) Range of 3MeV protons in W. The shaded area in green represents the investigation depth of semi constant damage before the Bragg peak.

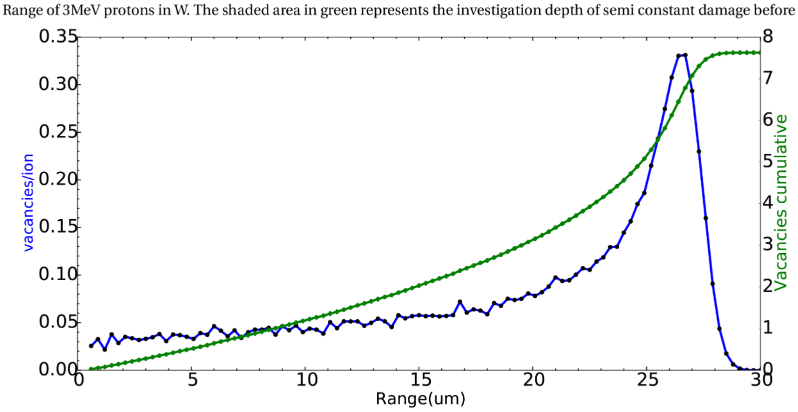

(b) Vacancy-range distribution(blue) and cummulative vacancies per ion(green) for 3MeV protons in W run on SRIM-2008.04[25].

Fig. 1. Proton range and vacancy distribution in W.

indentation is an extension of micro–hardness, wherein an indent is made on the material using spherical or pyramidal indenter. Applied force and displacement are measured during the indentation from which micro–hardness and elastic modulus are determined. This pilot study outlays the first irradiation and indentation of 'W' samples using the 3 MeV tandem accelerator and compares them to the self ion irradiations. The greater penetration depth of protons relative to self-ions allowed post irradiation indentation to be performed using both micro- and macro-indentation. The pilot experiment combines mechanical and retention investigations which are published separately [25]. These experiments form the basis for further high temperature investigations into using protons to induce irradiation damage.

2. Experiment

This study used 3 MeV protons to investigate irradiation hardening of tungsten. The penetration depth for 3 MeV protons was calculated to be 27 µm in tungsten samples as shown in Fig. 1. The calculations show that the Bragg peak which lies between 22 and 26 µm is preceded by an region of semi-constant damage levels of approximately 15 µm (shown in green in Fig. 1. In this semi-constant damage region of 15 µm, the vacancies per ion created by the proton can be approximated as a linear increase with depth ($2 \times 10^{-3}/\mu$ m+ 0.0277). This linear increase is also seen in the cumulative vacancies rise with depth in sub Fig. 1(b), subsequent to which an increase in slope and deviation from the linear behaviour is observed. The range of semi-constant damage was the maximum depth of all irradiation investigations within this work. The damage dose was calculated for 15 µm, as this is the maximum depth probed by macro-indentation. The depth of 15 µm would penetrate anywhere between 1 and 3 grains. The damage calculations for irradiation dose were performed using the quick calculation setup on SRIM-2008 [26] with a displacement threshold of 90 eV [27] in accordance with the technique prescribed by Stoller et al. [28]. However in view of restricting the damage to 15 µm, the integral target vacancies were considered and substituted in Eq. 1 as displacements per ion(DPI).

$$DPA = \frac{D}{R\rho S} \times DPI \tag{1}$$

Considering the total ion dose D, bombarded onto a spot size S, on a sample with atomic material density ρ, Eq. 1, would provide the net dpa damage dose for 15 µm of irradiated area.

Irradiations were performed using the tandem accelerator located on campus at Forschungszentrum Jülich. The tandem is capable of accelerating protons to 3.4 MeV(1.7 MV $\times$ 2), however the proton energies were limited to 3.0 MeV, below the threshold energy of (p,xn) reactions. JENDL/HE-2007 [29] extrapolates the cross-section to 100 µbarn for the (p,n) reaction on ^{186}W at 3 MeV proton energy and these are similar for ^{184}W. This is sufficiently low so as to avoid significant activation but at higher proton energies a build-up of nuclides would lead to radioactive inventory and potential release issues.

The irradiation chamber was specially designed for micro spots and contains a nano manipulator sample holder with a 10 nm resolution. It is also capable of performing nuclear reaction analysis and Rutherford backscattering analysis. The samples are loaded onto the manipulator in a sample holder and brought into the view of protons by controlled step motion. The focussing magnets prior to the irradiation chamber consist of a tunable triple quadrupole magnet system which allows focus spots having dimensions between 150 x 150 µm to 2 x 2 mm, from a normal beam diameter of 10 mm. A secondary electron suppression biased pico ampere-meter measured the proton dose onto the sample and the entire irradiation can be viewed from a tele-centric observation camera. A K type thermocouple measures the temperature at the back of the sample during irradiation.

The samples were cut using the electro discharge machining method from a bar stock of 99.95% chemically pure, sintered and double forged

Table 1
Irradiation parameters for each spot detailing the total accumulated charge, spot size, average proton current and calculated dpa.

Spot No	Total charge (μC)	Beam spot (μm)	Average current (nA)	dpa	Sample
1	1070	200 × 220	280	0.2	
2	4270	200 × 220	500	0.8	
3	2135	200 × 220	600	0.4	W_lowQ
4	1070	200 × 220	600	0.2	
5	5451	440 × 440	600	0.2	
6	9885	440 × 440	500	0.36	
7	5950	400 × 310	550	0.35	
1	980	240 × 310	570	0.1	
2	100	240 × 310	530	0.01	
3	300	240 × 310	547	0.03	*W_highQ*
4	1970	240 × 310	573	0.2	
5	2950	180 × 180	556	0.67	
6	1539	180 × 180	444	0.35	
7	5250	300 × 250	600	0.51	
1	7600	300 × 300	640	1.0	
2	3800	300 × 300	470	0.5	Recry_W
3	760	300 × 300	500	0.1	

W made by Plansee Group. The sample measures 10 × 10 mm in cross-section and is 5 mm thick. The surface was polished to a mirror finish with a surface roughness (Ra) of 90 nm prior to irradiation.

The samples were irradiated with beam spots between 180 and 400 µm diameter. The beam spot sizes were checked pre and post irradiation using scintillators and registered a deviation less than 4 pixels or 20 µm in either X or Y direction. Seven irradiations were carried out on the first 5 mm thick sample(W_lowQ). Each spot was separated from the others by a horizontal and vertical distance of 2 mm. Large blisters could be seen with the naked eye on the polished surface corresponding to the irradiation spots. Hence, a second sample (*W_highQ*) was irradiated with higher starting currents to achieve the same dose without blisters. The irradiation spot list with irradiation parameters is detailed in Table 1.

The ion beam analysis and nano manipulator restricted the temperature of the sample holder to a maximum of 333 K. Thus the only source of heating within the pilot experiment was limited to beam heating. Settings for higher temperatures are in progress. Calculations to estimate the temperature during irradiation was carried out using Ansys19.1. A starting heat flux of 2.1 W (700 nA current × 3 MeV) was projected onto a spot size of 300 µm × 300 µm on the 5 mm thick sample, with an initial temperature of 295 K. The temperature at the heat sink (back face of the sample) was limited to a maximum of 333 K from actual temperature measurements during the experiments. Radiative cooling was considered to be negligible at these temperatures and was removed from the calculations. A steady state calculation in Ansys resulted in the solution as shown in Fig. 2. The cut hemispherical beam spot overview shows that the thermal heat loading of 3 MeV protons as a source induced a steady state irradiation temperature of 360 K, which falls to within ± 3 K of background temperature at distance of 1.0 mm from the spot centre.

Lastly, three irradiations were carried out on a recrystallised tungsten sample for TEM measurements. TEM analysis was performed using Tecnai G2 F20 field emission microscope [30] at an acceleration voltage of 200 kV. The TEM was equipped with a double-tilt sample holder for precise sample orientation in order to visualise proton irradiation defects. TEM lamellas were prepared using a lift-out technique employing field emission scanning electron microscope(FE-SEM)[Zeiss Crossbeam540] equipped with a focussed ion beam FIB. The size of the lamella was 7 × 6 µm and final thickness of about 80 nm. The thinning of the lamella was performed in a 3 step process employing 30 kV ion beam with 700 nA, 100 nA and 20 nA current and a holder over tilt of ± 0.7°.

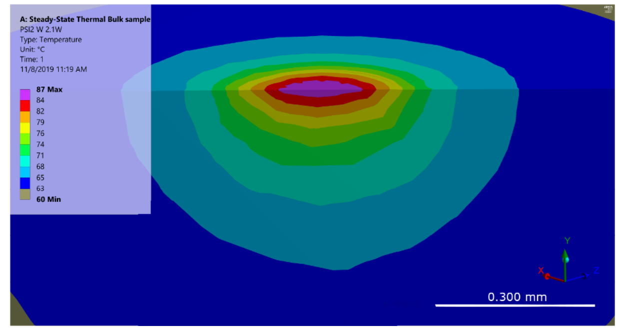

Fig. 2. Steady state heat flux simulation on Ansys19.1 showing an irradiation temperature of 360 K at the beam spot for sample W_low Q. The heat load from 3 MeV protons is seen to decay within ± 3 K of background temperature in 1 mm distance from the centre.

3. Results

3.1. Blister formation

Blisters were observed after irradiation on sample W_lowQ. These blisters were large enough to be seen with the naked eye and corresponded to the beam spot size from the irradiations. Optical profilometry using a scanning confocal microscope (Micromeasure 2 from Stil SA) was performed on the sample. This technique uses white light and avoids contact with the sample surface. The blisters were clearly seen using this technique. Optical profilometry image of the sample with a high resolution blister profile is shown in Fig. 3a. The change in colour (green spots) in Fig. 3a represents a height difference on the surface of the sample which corresponds to the irradiated spots. An altitude line scan of the first three spots is shown in Fig. 3b. The altitude scan portrays a direct co-relation between dose and blister height for spot 1, spot 2 and spot 3, although this relation doesn't hold for all spots. The maximum blister height measured was 27 µm at 0.8 dpa. From the gauss like shape of the altitude measurements in Z-X and Z-Y dimensions, the blister seems to resemble the double gauss irradiation beam profile. A High resolution intensity and altitude scan for blister spot 1 is seen in Fig. 4. The 3 dimensional recreation of the blister shows cracks which seem to originate from the centre of the blister. A crack network is seen on the surface of the blister in Fig. 4a.

These blisters rendered W_lowQ unsuitable for micro indentation, with attempted measurements giving abnormal modulus and hardness results. However, it was found that the formation of blisters could be suppressed by increasing the initial beam current. This enabled hardness testing of *W_highQ* (see Section 3.3). The blisters in W_lowQ appear to have been caused by a large cavity opening up at a depth close to that of the expected Bragg peak as shown in Fig. 8a. The formation of this cavity was suppressed by the higher initial beam current in *W_highQ* (Fig. 8b).

3.2. Transmission electron microscopy

Transmission electron microscopy(TEM) was performed on irradiated spot lift-outs made from FIB cuts. The lift-outs were cleaned using a 30 kV Ga focused ion beam (FIB) until they appeared transparent under a 10 kV electron beam and then cleaned using a 5 kV Ga FIB beam. Fig. 5 shows a series of TEM images for increasing dose of irradiation. The damage induced while using FIB for cutting and cleaning of the lamella is seen on the first left image(0 dpa). At 0.1 dpa some dislocations were observed distinct from the background 'black-dot' FIB image. These loops are better seen in the following picture corresponding to 0.5 dpa damage and continued to increase up to 1 dpa. The loops are uniformly distributed and tend to increase in diameter. No voids are seen in the images through the use of under and

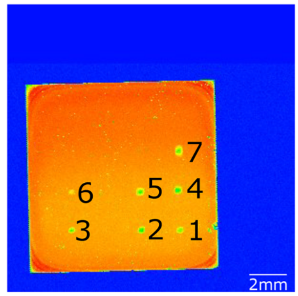

(a) 7 distinct irradiation spots in green seen on the sample using surface scan optical profilometry on a confocal microscope.

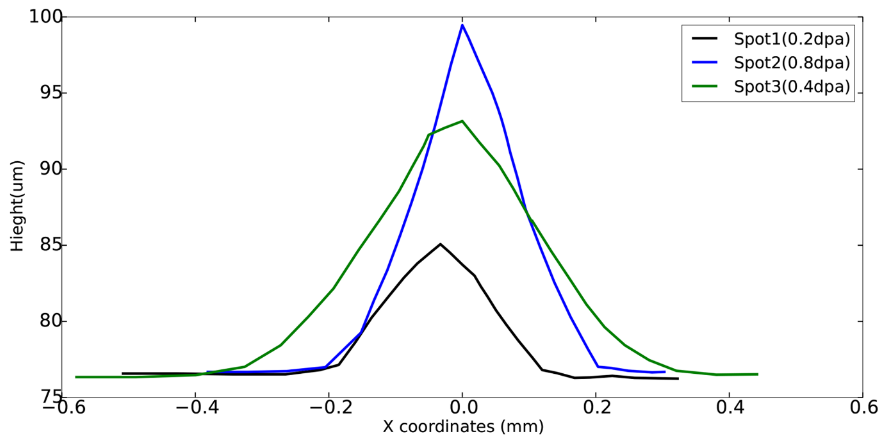

(b) Altitude line scan of spot1, 2 and 3 shows that the blister height relates to dose.

Fig. 3. Optical profilometry picture of irradiated sample W_lowQ.

over focus method. Given the clarity of the images from 0.5 and 1 dpa samples, this was considered to rule out the formation of voids > 5 nm under these irradiation conditions.

Loop density and size investigations were performed. Images having on average sizes of 130 × 207 nm were analysed for doses of 0.1, 0.5 and 1 dpa. The images were analysed using ImageJ software [31]. Each image was first inverted and then analysed for maxima (loop density counts) using the grey scale reduction technique described in [32]. A loop density of 2.2×10^{23} m^{-3}, 1.5×10^{23} m^{-3} and 1.8×10^{23} m^{-3} was counted for 0.1, 0.5 and 1.0 dpa respectively. The background noise, particularly for 0.1 dpa image results in large uncertainity. However, the loop density did not seem to drastically increase between 0.5 and 1.0 dpa which could point to saturation below 0.5 dpa. This is a contradiction to the self ion irradiated results of 150 keV energy [32], where a steady increase of loop density with dose was observed, but is consistent with the self ion 2 MeV energy irradiation results from Armstrong et al. [33], where ”little difference” was found in loop density for 0.4 dpa and 1.2 dpa dose. It is also consistent with in situ proton irradiation of tungsten [18] where a decrease in loop density with increasing dose up to 0.3 dpa was observed and no change in loop

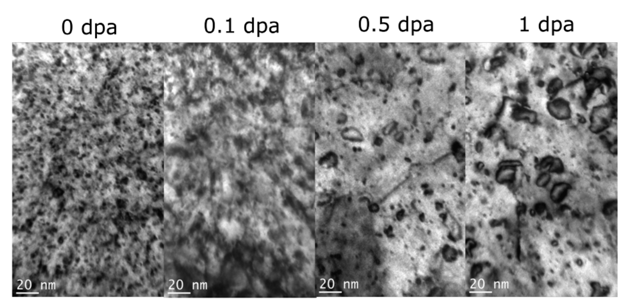

Fig. 5. Progressive dose level based TEM images for proton irradiated tungsten. An increase in loop diameter is noticed.

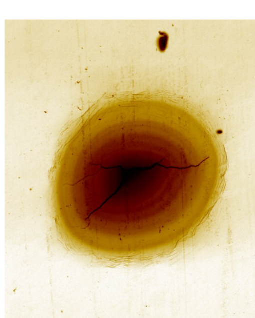

(a) W5mm_1 Spot1 blister intensity image scan on which cracks are clearly seen.

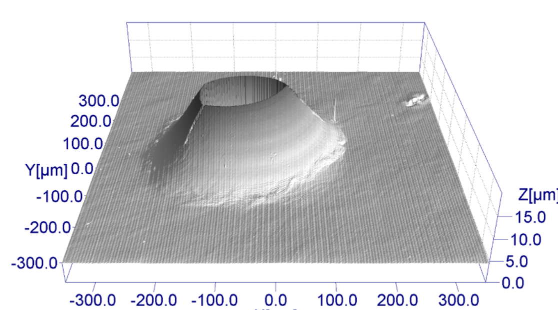

(b) 3D recreation of the Spot1 blister. A height of 15μm for the blister is seen with a good co-relation to the beam spot size.

Fig. 4. High resolution intensity and altitude scan of W_lowQ Spot 1 blister.

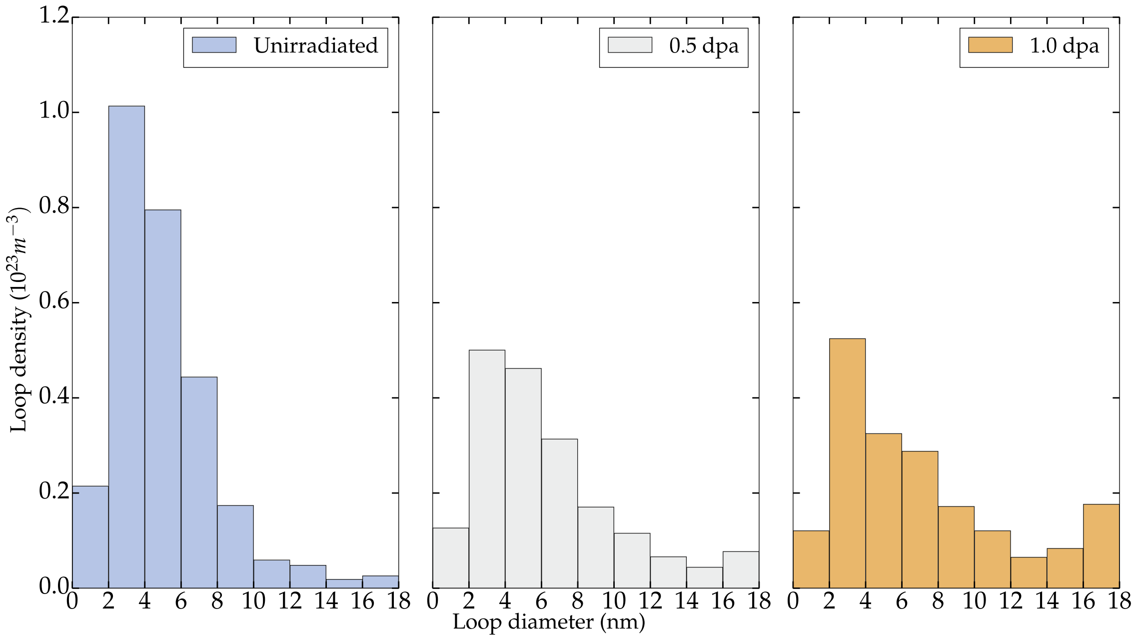

Fig. 6. Loops size density histograms for un-irradiated(blue), 0.5(grey) and 1.0(orange) dpa 3 MeV proton irradiated tungsten. The density of loops is grouped into intervals of 2 nm for which the bars represent the number of loops(x10^{23}) per m^3 within that interval. The last bin includes all diameters larger than 16 nm.

density was found between 0.3 and 0.7 dpa.

Histograms with loop diameter sizes between 0 and 18 nm binned at 2 nm intervals for unirradiated, 0.5 and 1.0 dpa are shown in Fig. 6. The last bin includes all diameters > 16 nm. The images were analysed using particle finder option in ImageJ after converting it to binary as described in [32]. The loop diameter shown represents the major diameter resulting from the best fit ellipse method. The unirradiated images showed higher FIB damage than 0.5 and 1.0 dpa. With increasing dose the number density of small sized loops decreases, while the loop density for large sized loop increases. There was a steady rise in density of loops > 10 nm with dose. This correlates well with the earlier TEM images in Fig. 5, where with increasing dose larger loops are seen to appear. Although we did not measure the Burgers vectors of these loops, from previous literature [18] [12], it is highly likely that the vast majority of these loops are < 111 > -type, since < 100 > -type loops are unstable in size [12].

3.3. Hardness testing – micro vs macro indentation

As the range of investigation in 3 MeV proton irradiated tungsten is 15 µm, both micro and macro indentation were performed on the irradiation spots for sample *W_highQ* at room temperature. Micro indentation was performed using a diamond Berkokvich indenter tip on a Agilent G200 Nanoindenter. The micro indentation was carried out using the continues stiffness measurement(CSM) technique [34] at a strain rate of 0.05 s^{-1} to a depth of 2 µm. The required inputs for micro indentation are listed under Table 2. All indents were arranged in a 5 × 5 array on the beam spot. The spacing between any two indents was 20 µm which follows the ISO norm for 10x the maximum indent depth in order to avoid mutual influence. Initial calibration of the diamond tip was done on a fused silica sample which was used to set the machine frame stiffness. Each indent produced a force displacement and a hardness displacement curve. Indentation hardness was derived for each spot by averaging the values from CSM between 500–1500 nm depth. This was done in order to avoid surface effects like polishing influencing the results. The error was considered as the standard error in the hardness from 25 indents on each spot.

Macro-indentation was carried out on the same spots using a Zwiki ZHU0.2 on the sample *W_highQ*, to achieve a direct comparison. A pyramidal diamond tip Vickers indenter was used and each indent was 100 x 100 µm on average. The order of magnitude greater depth ensured that the damage induced by prior micro-indentation would not influence the result. Machine compliance measurements for stiffness correction were undertaken using a series of indents from 1 to 16 N on a 316L steel sample. Mono cyclic loading up at 0.133 N/s to a maximum of 15 N was performed with a holding time of 10 s at max load. Load displacement curves were recorded during the indentation and further analysed according to the standard DIN EN ISO14577 [35]. A Levenberg–Marquardt (least square) fit [36] was applied to 95–50% of the unloading load displacement curve. Major input parameters and fit data used to calculate indentation hardness are given in Table 3.

The comparison of indentation hardness values obtained from the two methods on the same irradiation spots is shown in Fig. 7. Both indentation methods show a similar characteristic of early onset of hardness increase and quick saturation. A jump of 0.8 GPa in hardness is seen for the first step of 0.01 dpa. A further increase of 0.5 GPa in case of micro-indentation and 1 GPa in the case of macro indentation occurs between 0.01 and 0.03 dpa. This was found to be the saturation dose beyond which no further substantial increase in hardness was observed. 7 GPa was the saturation value for indentation hardness. 25

Table 2
Inputs for micro indentation of irradiated samples.

Input	Value
Maximum depth	2000 µm
Frequency target	45 Hz
Strain rate	0.05 s^{-1}
Harmonic displacement target	2 nm

Table 3
Inputs for macro-indentation of irradiated samples

Input	Value
Speed of load application	0.133 N/s
Holding time at max load	10 s
Load removal speed	2 N/s
Portion of curve fit	95–50%

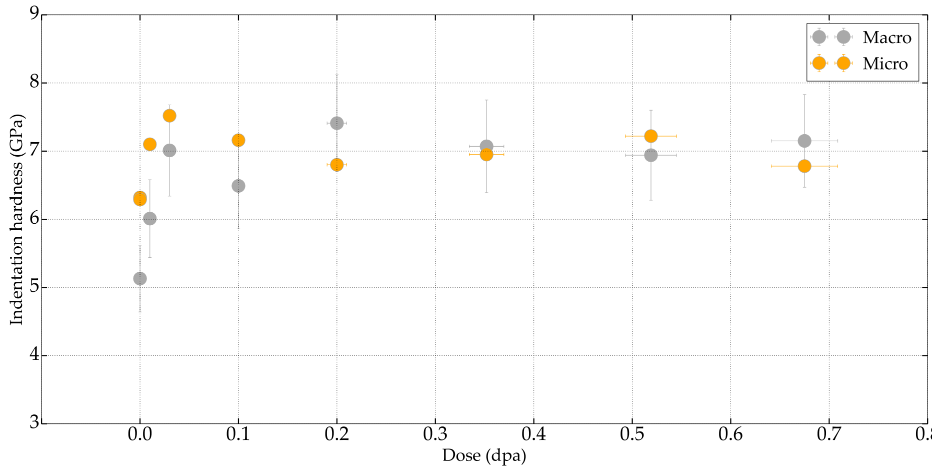

Fig. 7. Hardness measurement comparisons between micro and macro indentation methods.

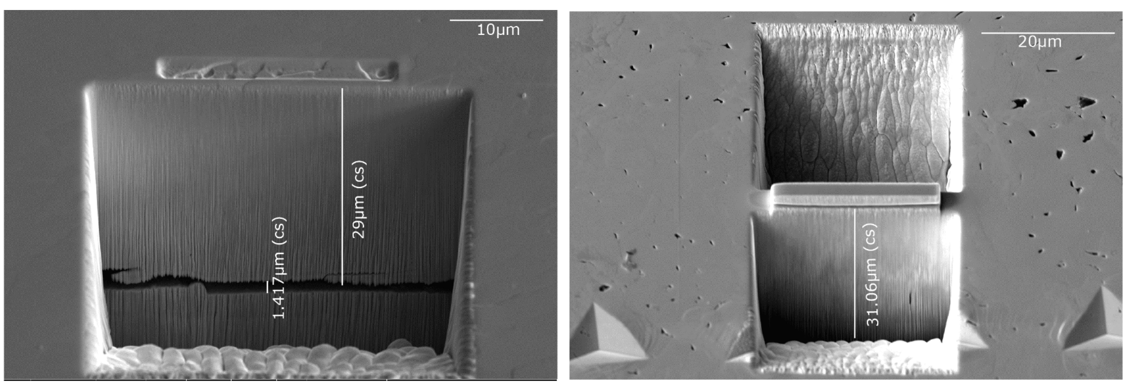

(a) FIB cut on spot1 W_lowQ (0.2 dpa)

(b) FIB cut on spot3 *W_highQ* (0.03 dpa)

Fig. 8. FIB cut on sample W_lowQ which shows a large void just past the Bragg peak, which isn't seen in sample *W_highQ*.

micro-indents and one macro indent was carried out for each spot. A maximum error of 10% was calculated from the fluctuations of results from indents on an un-irradiated region of the sample.

4. Discussion

The large blisters prevented indentation studies on proton damaged sample W_lowQ (see Section 3.1). Similar blisters have been observed in a recent study [37], where they propose that high penetration depths which prevent the escape of hydrogen from the surface are responsible for the blister formations at lower fluxes. Further research into the dependence of blisters on dose and flux has been conducted by Segev et al. [38] and has found a threshold dose at 3×10^{17} protons/cm^2 for polycrystalline W. This threshold dose for blister formation was understood to be independent of irradiation temperature in the case of polycrystalline W samples.

However using a higher starting beam current was seen to suppress blistering in this work. Also, considering the similarity between the beam profile and blister pattern, we are of the opinion that blister growth is irradiation dependent. In particular, the blisters start to grow rapidly on cold samples (295 K) upon commencement of the irradiation, with the height increase slowing as the irradiation progresses. Thus, by starting with a high beam current which was gradually lowered to achieve the desired current and dose, blister formation and growth were suppressed. A very high current at the start offsets the cold sample temperature and prevents the rapid ingrowth of the blister at the start of the irradiation. This has worked successfully on sample *W_highQ*, where blistering wasn't noticed for the irradiation spots even at doses of 2.5×10^{19} protons/cm^2.

From experiments with plasma [39–41], we understand that the diffusion plays a dominant role towards hydrogen/proton retention in tungsten. In fact from experiments, hydrogen/protons are known to travel several μm with low energy plasma exposures [40,41]. Protons in tungsten have relatively high diffusion coefficient [42] ($D_F = 4.1 \times 10^{-07}$ m^2/s) scaling exponentially with temperature and thus, in effect a high diffusion length. At the low initial temperature (295 K), it is likely that the protons diffuse into damage-induced cavities near to the Bragg peak and these cavities grow to form a large bubble as seen in the FIB cut in Fig. 8. The large bubble pushes material upwards and is responsible for the blistering along with the cracks. With high starting currents, as in *W_highQ*, the temperature rise in the Bragg peak is much quicker, resulting in the protons diffusing away from the Bragg peak further into the bulk and preventing cavity formation. This conclusion is backed up by the appearance of a large cavity near the Bragg peak in W_lowQ and no such cavity being present in *W_highQ* (Fig. 8). A contradiction to the reported work of Segev et al. [37] could be due to the differences in irradiation surface to volume ratio between the experiments. With a highly focussed beam of 400 × 400 μm as in the case of our experiments, diffusion into the bulk, in the lateral direction would be considerably higher as compared to a beam spot of 5 × 5 mm, where the local void filling is more likely. Although there is the possibility that the blister exists however is too small to be seen. Further experiments using samples heated to a steady stage temperature by a stage heater rather than beam heating could be carried out to confirm this result.

The cracks formed on top of the blister surface for sample W_lowQ were investigated using scanning electron microscopy(SEM) techniques. Shown in Fig. 9 is a blister on irradiation spot 2 and 3, sample

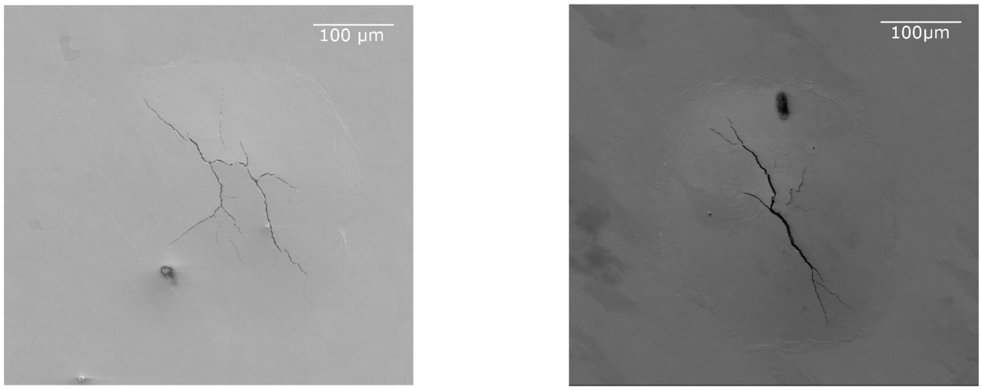

(a) SEM image of the irradiation spot2 on sample W_lowQ

(b) SEM image of the irradiation spot3 on sample W_lowQ

Fig. 9. SEM pictures of irradiated spot.

W_lowQ. The large cracks are seen to be up to 2 µm thick running along the irradiated area. Focussed ion beam cuts on the cracks reveal a crack network into the sample exceeding 5 µm. A black coating was noticed on the sample surface and found to be proton assisted carbon deposition. The carbon deposition persists in spite of vacuum conditions of 1×10^{-07} mbar in the irradiation chamber. Using nuclear reaction analysis, the carbon & oxygen layer was found to have a thickness of 5 nm and hence, will not induce any macroscopic changes in the sample.

Hardness measurement could only be carried out on the unblistered sample (*W_highQ*). As expected micro-indentation shows a higher hardness in the unirradiated sample than macro-indentation. This is due to the size effect descrbed by Nix and Gao [43]. At higher doses this difference appears to disappear, which could indicate a change in size effect with increasing irradiation hardening, however due to the large uncertainty in the macro indentation results, where only one indent per spot was possible, no strong conclusions can be drawn. Irradiation hardening was observed to saturate using both techniques at 0.03 dpa. This contrasts with TEM results where loop size continues to grow with increasing dose, while loop density remains approximately constant. Previous work performed by Hu et al. [44] has considered dislocation loops as weak obstacles as opposed to voids and precipitates which are strong obstacles to dislocation plane motion and could explain the saturation in irradiation hardening. From TEM observations as shown in Fig. 5, we note the presence of only dislocation loops. The formation of dislocation loops starts early and leads to a jump in hardness. With saturation towards the number density of loops a saturation in hardness is seen. Dislocation loop number density seems to play a much higher role as compared to dislocation size for hardness. As no voids or precipitates are noticed, no further increase in irradiation hardening is observed. Although, an Orowan based hardening model would suggest that the irradiation hardening caused by dislocation loops depends strongly on loop size. Further work is required to understand why that is not observed here.

Recent fission irradiation studies conducted at HFIR have noted that no strong co-relation between irradiation hardness and irradiation temperature was noticed for tungsten samples [44,45]. However, given the low irradiation temperatures in this study, a comparison is attempted between macro indentation results from this work, HFIR results at 363 K irradiation temperature [45,44] and self ion irradiation measurements [33] at 573 K which is plotted in Fig. 10. Fission irradiation hardness measurements are based on the Vickers hardness testing method while the self ion irradiation results were obtained using a Berkovich indenter and continues stiffness method.

Fission neutron irradiations on W induce a combination of dislocations and voids at temperatures < 1073 K for damage dose under 1 dpa [46]. Thus a hardening is observed for a low dose of 0.004 dpa damage [45]. In fact Hu et al. attributed the initial hardening to initiation and saturation of dislocation loops and voids [44]. Upon further irradiation, a void lattice is known to develop and which thereafter changes to a mixture of voids and W-Re precipitates [47] [46]. W-Re precipitates are formed through transmutation and are neutron spectrum dependent [48]. They are observed to grow with dose and result in increasing the irradiation hardening beyond 1 dpa [44,45]. Such a jump in irradiation hardening is also seen in Fig. 10. Self ion irradiations were observed to introduce only dislocation loops in W. They displayed a similar hardening behaviour as the 3 MeV proton irradiated samples. Armstrong et al. reported an increase of 0.8 GPa for irradiation to 0.4 dpa that then saturates [33]. This correlates well with the saturation in loop density observed by the authors. In this work we also observe a saturation of irradiation hardness with steady dislocation loop density. Devoid of any further barrier for dislocation slip, no hardening is noticed.

Further work is required to demonstrate how self-ion or proton irradiation can be used to mimic this precipitation behaviour in order to produce realistic irradiation hardening levels. Armstrong et al. measured the hardness post 2 MeV self ion irradiation with He ion irradiation and observed large hardness increase, however no bubbles were observed in the TEM [49]. Armstrong et al. also noted the rise of irradiation hardening in W-5Re alloy at 33 dpa, 2 MeV self ion damage from clustering of Re atoms [33]. Xu et al. irradiated W-2Re and W-1Re-1Os alloys with 2 MeV self ions and also observed clustering [17]. However, the needle like precipitation and accompanying hardness changes seen from fission irradiations [50] evades ion irradiations. Recently Harrison et al. showed the production of needle like precipitates using 350 keV Ne ion irradiation in W-26Re alloy at 773 and 1073 K [51]. Another potential area of interest is utilising high energy protons (> 10 MeV) to induce transmutation as per dpa rates expected in a fusion environment [21].

5. Summary

Irradiation damage in tungsten was tested in a pilot experiment using 3 MeV protons and the irradiation hardening quantified using micro- and macro-indentation. Concentrated beam spots of sizes below 1 mm were used to achieve dose rates between 1×10^{-04} and 5×10^{-05} dpa/s. The dose rates are comparable to the self ion damage rates of 8×10^{-04} dpa/s [33] and has allowed for irradiation damage levels of up to 0.7 dpa. Protons have a larger penetration depth as compared to heavy ions and penetrate to 27 µm depth in W, generating defects on a macroscopic scale. Large blisters were observed on the irradiation spots, however, their formation was suppressed by utilising a high initial beam current.

Samples irradiated to 0.01–0.7 dpa dose were investigated using

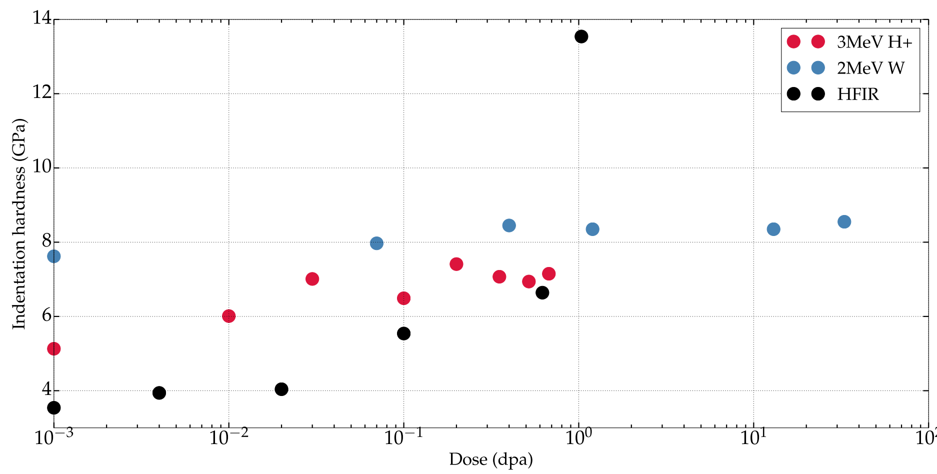

Fig. 10. Hardness comparison from protons, self ions[33] and fission neutrons (0.003& 0.02dpa [45], 0.6dpa [44]).

nano- and macro-indentation techniques. The irradiation hardening was observed to saturate at ≈ 1 GPa at 0.03 dpa. This was similar to the behaviour observed using self-ion irradiation [33] but contrasted strongly with fission neutron irradiations where hardening was observed to increase beyond 1 dpa [45].

TEM observations were carried out for irradiation spots of 0.1, 0.5 and 1 dpa dose to determine the microstructural changes induced by proton damage. Dislocation loops were detected at 0.1 dpa dose and grew in size with increasing dose. A dislocation loop density of 1.8×10^{23} loops/m^3 for 1 dpa and 360 K was calculated against 4×10^{22} loops/m^3 at 1.2 dpa and 773 K [32] for self ions and 3.3×10^{22} loops/m^3 for 1 dpa at 773 K from neutron irradiations [45].

CRediT authorship contribution statement

R. Rayaprolu: Conceptualization, Methodology, Formal analysis, Investigation, Visualization, Writing - original draft, Writing - review & editing. **S. Möller:** Conceptualization, Methodology, Writing - review & editing, Supervision. **R. Abernethy:** Investigation, Formal analysis, Writing - review & editing. **M. Rasinski:** Investigation. **J.C. Haley:** Investigation, Formal analysis, Writing - review & editing. **Ch. Linsmeier:** Methodology, Resources, Supervision.

Declaration of Competing Interest

The authors declare that they have no known competing financial interests or personal relationships that could have appeared to influence the work reported in this paper.

Acknowledgement

The authors would like to acknowledge the support of HiTEC graduate school and thank B.Göths for her kind assistance during the electron microscopy work. This study used UKAEA's Materials Research Facility, which has been funded by and is part of the UK's National Nuclear User Facility and Henry Royce Institute for Advanced Materials [Grant No. EP/P021727/1]. This work has been supported by the RCUK Energy Programme [Grant No. EP/P012450/1] and EPSRC [Grant No. EP/N017854/1 and EP/P001645/1]. It has been carried out within the framework of the EUROfusion Consortium and has received funding from the Euratom research and training programme 2014–2018 and 2019–2020 under Grant Agreements No. 633053. The views and opinions expressed herein do not necessarily reflect those of the European Commission.

References

[1] D. Maisonnier, I. Cook, Sardain Pierre, Boccaccini Lorenzo, Bogusch Edgar, Broden Karin, Di Pace Luigi, Forrest Robin, Giancarli Luciano, Hermsmeyer Stephan, Nardi Claudio, Norajitra Prachai, Pizzuto Aldo, Taylor Neill, and Ward David. The european power plant conceptual study. Fusion Engineering and Design, 75–79:1173–1179, Nov 2005.
[2] M.R. Gilbert, T. Eade, C. Bachmann, U. Fischer, N.P. Taylor, Activation, decay heat, and waste classification studies of the european DEMO concept, Nucl. Fusion 57 (4) (Mar 2017) 046015.
[3] Mohamed Abdou, Neil B. Morley, Sergey Smolentsev, Alice Ying, Siegfried Malang, Arthur Rowcliffe, Mike Ulrickson, Blanket/first wall challenges and required r&d on the pathway to demo, Fusion Eng. Des. 100 (2015) 2–43.
[4] M. Wirtz, I. Uytdenhouwen, V. Barabash, F. Escourbiac, T. Hirai, J. Linke, Th. Loewenhoff, S. Panayotis, G. Pintsuk, Material properties and their influence on the behaviour of tungsten as plasma facing material, Nucl. Fusion 57 (6) (Apr 2017) 066018.
[5] Takeshi Miyazawa, Taehyun Hwang, Kohei Tsuchida, Takaya Hattori, Makoto Fukuda, Shuhei Nogami, Akira Hasegawa, Effects of helium on mechanical properties of tungsten for fusion applications, Nucl. Mater. Energy 15 (May 2018) 154–157.
[6] Chen-Hsi Huang, Mark R. Gilbert, Jaime Marian, Simulating irradiation hardening in tungsten under fast neutron irradiation including re production by transmutation, J. Nucl. Mater. 499 (Feb 2018) 204–215.
[7] H. Bolt, V. Barabash, W. Krauss, J. Linke, R. Neu, S. Suzuki, N. Yoshida, ASDEX Upgrade Team. Materials for the plasma-facing components of fusion reactors. J. Nucl. Mater., 329–333:66–73, 2004.
[8] Michael Rieth, Russell Doerner, Akira Hasegawa, Yoshio Ueda, Marius Wirtz. Behavior of tungsten under irradiation and plasma interaction. J. Nucl. Mater., 519:334–368, 2019.
[9] J. Knaster, A. Moeslang, T. Muroga, Materials research for fusion, Nat. Phys. (May 2016) 424–434.
[10] L.M. Garrison, Y. Katoh, N.A.P. Kiran Kumar, Mechanical properties of single-crystal tungsten irradiated in a mixed spectrum fission reactor, J. Nucl. Mater. 518 (2019) 208–225.
[11] R.G. Abernethy, Predicting the performance of tungsten in a fusion environment: a literature review. jun, Mater. Sci. Technol. 33 (4) (2016) 388–399.
[12] R.W. Harrison, On the use of ion beams to emulate the neutron irradiation behaviour of tungsten, Vacuum 160 (Feb 2019) 355–370.
[13] A. Ibarra, F. Arbeiter, D. Bernardi, M. Cappelli, A. García, R. Heidinger, W. Krolas, U. Fischer, F. Martin-Fuertes, G. Micciché, A. Muñoz, F.S. Nitti, M. Pérez, T. Pinna, K. Tian, The IFMIF-DONES project: preliminary engineering design, Nucl. Fusion 58 (10) (Aug 2018) 105002.
[14] Steven J. Zinkle, Anton Mslang, Evaluation of irradiation facility options for fusion materials research and development, Fusion Eng. Des. 88 (6–8) (Oct 2013) 472–482.
[15] D.E.J. Armstrong, A.J. Wilkinson, S.G. Roberts, Mechanical properties of ion-implanted tungsten-5wt% tantalum, Phys. Scr. T145 (Dec 2011) 014076.
[16] O.V. Ogorodnikova, V. Gann, Simulation of neutron-induced damage in tungsten by irradiation with energetic self-ions, J. Nucl. Mater. 460 (May 2015) 60–71.
[17] Xu. Alan, Christian Beck, David E.J. Armstrong, Krishna Rajan, George D.W. Smith, Paul A.J. Bagot, Steve G. Roberts, Ion-irradiation-induced clustering in w-re and w-re-os alloys: a comparative study using atom probe tomography and nanoindentation measurements, Acta Mater. 87 (Apr 2015) 121–127.
[18] I. Ipatova, R.W. Harrison, P.T. Wady, S.M. Shubeita, D. Terentyev, S.E. Donnelly, E. Jimenez-Melero, Structural defect accumulation in tungsten and tungsten-5wt.% tantalum under incremental proton damage, J. Nucl. Mater. 501 (Apr 2018) 329–335.
[19] G.S. Was, J.T. Busby, T. Allen, E.A. Kenik, A. Jensson, S.M. Bruemmer, J. Gan, A.D. Edwards, P.M. Scott, P.L. Andreson, Emulation of neutron irradiation effects

with protons: validation of principle, J. Nucl. Mater. 300 (2–3) (2002) 198–216.
[20] Gary S. Was, Fundamentals of Radiation Material Science, Springer-Verlag, Berlin Heidelberg, 2010.
[21] R. Rayaprolu, S. Mller, Ch. Linsmeier, S. Spellerberg, Simulation of neutron irradiation damage in tungsten using higher energy protons, Nucl. Mater. Energy 9 (Dec 2016) 29–35.
[22] P. Jung, A. Hishinuma, G.E. Lucas, H. Ullmaier, Recommendation of miniaturized techniques for mechanical testing of fusion materials in an intense neutron source, J. Nucl. Mater. 232 (2–3) (1996) 186–205.
[23] G.E. Lucas, G.R. Odette, M. Sokolov, P. Sptig, T. Yamamoto, P. Jung, Recent progress in small specimen test technology, J. Nucl. Mater. 307–311 (Dec 2002) 1600–1608.
[24] G.E. Lucas, G.R. Odette, H. Matsui, A. Möslang, P. Spätig, J. Rensman, T. Yamamoto, The role of small specimen test technology in fusion materials development, J. Nucl. Mater. 367–370 (2007) 1549–1556.
[25] S. Moeller, R. Krug, R. Rayaprolu, B. Kuhn, E. Joußen, A. Kreter, Deuterium retention in tungsten and reduced activation steels after 3 MeV proton irradiation, Nucl. Mater. Energy 23 (2020) 100742.
[26] J.F. Ziegler, Stopping of energetic light ions in elemental matter, J. Appl. Phys. 85 (3) (1999) 1249–1272.
[27] Standard practice for neutron radiation damage simulation by charged-particle irradiation. Technical report, West Conshohocken, PA, 1996. Reapproved 2009.
[28] R.E. Stoller, M.B. Toloczko, G.S. Was, A.G. Certain, S. Dwaraknath, F.A. Garner. On the use of SRIM for computing radiation damage exposure. Nucl. Instruments Methods Phys. Res. Section B: Beam Interactions Mater. Atoms, 310:75–80, 2013.
[29] Y. Watanabe, K. Kosako, S. Kunieda, S. Chiba, R. Fujimoto, H. Harada, M. Kawai, F. Maekawa, T. Murata, H. Nakashima, K. Niita, N. Shigyo, S. Shimakawa, N. Yamano, T. Fukahori, Status of JENDL high energy file, J. Korean Phys. Soc. 2 (3) (2011) 1040–1045.
[30] Martina Luysberg, Marc Heggen, Karsten Tillmann, FEI tecnai g2 f20, J. Large-Scale Res. Facilities JLSRF 2 (2016).
[31] Caroline A. Schneider, Wayne S. Rasband, Kevin W. Eliceiri, NIH image to ImageJ: 25 years of image analysis, Nat. Methods 9 (7) (2012) 671–675.
[32] Xiaoou Yi, Michael L. Jenkins, Khalid Hattar, Philip D. Edmondson, Steve G. Roberts. Characterisation of radiation damage in w and w-based alloys from 2 MeV self-ion near-bulk implantations. Acta Materialia, 92:163–177, jun 2015.
[33] D.E.J. Armstrong, X. Yi, E.A. Marquis, S.G. Roberts, Hardening of self ion implanted tungsten and tungsten 5-wt% rhenium, J. Nucl. Mater. 432 (1–3) (2013) 428–436.
[34] W.C. Oliver, G.M. Pharr, Measurement of hardness and elastic modulus by instrumented indentation: Advances in understanding and refinements to methodology, J. Mater. Res. 19 (01) (2004) 3–20.
[35] ISO/TC 164/SC 3 Hardness testing. Metallic materials - instrumented indentation test for hardness and materials parameters iso 14577–1:2015. Technical report.
[36] Matt Newville, Renee Otten, Andrew Nelson, Antonino Ingargiola, Till Stensitzki, Dan Allan, Austin Fox, Faustin Carter, Michał, Dima Pustakhod, Yoav Ram, Glenn, Christoph Deil, Stuermer, Alexandre Beelen, Oliver Frost, Nicholas Zobrist, Gustavo Pasquevich, Allan L.R. Hansen, Alexander Stark, Tim Spillane, Shane Caldwell, Anthony Polloreno, Andrewhannum, Jose Borreguero, Jonathan Fraine, Deep-42-Thought, Benjamin F. Maier, Ben Gamari, and Anthony Almarza. lmfit/lmfit-py 0.9.14. Technical report, 2019.
[37] I. Gavish Segev, E. Yahel, I. Silverman, and G. Makov. Blister formation at subcritical doses in tungsten irradiated by MeV protons. J. Nucl. Mater. , 496:77–84, 2017.
[38] I. Gavish Segev, E. Yahel, I. Silverman, A. Perry, L. Weismann, and G. Makov. Hydrogen blister formation in single crystal and polycrystalline tungsten irradiated by MeV protons. Journal of Nuclear Materials, Nov 2018.
[39] Rion A. Causet, Thomas J. Venhaus, The use of tungsten in fusion reactors: A review of the hydrogen retention and migration properties, Phys. Scr. T94 (1) (2001) 9.
[40] Joachim Roth, Klaus Schmid, Hydrogen in tungsten as plasma-facing material, Phys. Scr. T145 (2011) 014031.
[41] T. Tanabe, Review of hydrogen retention in tungsten, Phys. Scr. T159 (2014) 014044.
[42] R. Frauenfelder, Permeation of hydrogen through tungsten and molybdenum, J. Chem. Phys. 48 (9) (1968) 3955–3965.
[43] William D. Nix, Huajian Gao, Indentation size effects in crystalline materials: a law for strain gradient plasticity, J. Mech. Phys. Solids 46 (3) (Mar 1998) 411–425.
[44] Xunxiang Hu, Takaaki Koyanagi, Makoto Fukuda, N.A.P. Kiran Kumar, Lance L. Snead, Brian D. Wirth, Yutai Katoh. Irradiation hardening of pure tungsten exposed to neutron irradiation. J. Nucl. Mater., 480:235–243, Nov 2016.
[45] Y. Katoh, L.L. Snead, L.M. Garrison, X. Hu, T. Koyanagi, C.M. Parish, P.D. Edmondson, M. Fukuda, T. Hwang, T. Tanaka, A. Hasegawa, Response of unalloyed tungsten to mixed spectrum neutrons, J. Nucl. Mater. 520 (Jul 2019) 193–207.
[46] Akira Hasegawa, Makoto Fukuda, Kiyohiro Yabuuchi, Shuhei Nogami, Neutron irradiation effects on the microstructural development of tungsten and tungsten alloys, J. Nucl. Mater. 471 (Apr 2016) 175–183.
[47] Makoto Fukuda, Kiyohiro Yabuuchi, Shuhei Nogami, Akira Hasegawa, Teruya Tanaka, Microstructural development of tungsten and tungsten-rhenium alloys due to neutron irradiation in HFIR, J. Nucl. Mater. 455 (1–3) (Dec 2014) 460–463.
[48] Makoto Fukuda, N.A.P. Kiran Kumar, Takaaki Koyanagi, Lauren M. Garrison, Lance L. Snead, Yutai Katoh, Akira Hasegawa. Neutron energy spectrum influence on irradiation hardening and microstructural development of tungsten. J. Nucl. Mater., 479:249–254, 2016.
[49] D.E.J. Armstrong, P.D. Edmondson, S.G. Roberts. Effects of sequential tungsten and helium ion implantation on nano-indentation hardness of tungsten. Appl. Phys. Lett., 102(25):251901, 2013.
[50] Takashi Tanno, Akira Hasegawa, Jian-Chao He, Mitsuhiro Fujiwara, Shuhei Nogami, Manabu Satou, Toetsu Shishido, Katsunori Abe, Effects of transmutation elements on neutron irradiation hardening of tungsten, Mater. Trans. 48 (9) (2007) 2399–2402.
[51] R.W. Harrison, G. Greaves, J.A. Hinks, S.E. Donnelly, Intermetallic re phases formed in ion irradiated WRe alloy, J. Nucl. Mater. 514 (Feb 2019) 123–127.